JOURNAL OF MECHANICAL ENGINEERING AND SCIENCES (JMES)
ISSN: 2289-4659 e-ISSN: 2231-8380
VOL. 15, ISSUE 1, 7684 – 7694
DOI: https://doi.org/10.15282/jmes.15.1.2021.06.0606

ORIGINAL ARTICLE

Effect of friction stir welding parameters on the residual stress distribution of Al-2024-T6 alloy

Majid Farhang[1], Omid Sam-Daliri[1], Mohammadreza Farahani[1,*], Azadeh Vatani[2]

[1] School of Mechanical Engineering, College of Engineering, University of Tehran, Tehran, Iran
[2] Department of Mechanical, Industrial and Aerospace Engineering (MIAE), Concordia University, Montreal, Quebec, Canada

ABSTRACT – The objective of this study was to investigate the influences of the main parameters of friction stir welding (FSW) on the residual stresses remained in the FSW of Al 2024-T6. The main parameters were tool rotational speed and tool transverse speed. The effect of these parameters on the residual stresses was studied in both finite element simulation and hole drilling strain gauge measurement. The results showed a good agreement between the numerical results and the experimental outcomes. The change in transverse speed from 25 to 31.5mm/min resulted in increase of longitudinal residual stresses in welding centerline in which the longitudinal residual stress was increased at the tool rotational speed of 1120rpm and 1600rpm about 12.5% and 2.67%, respectively. The results showed that at the low rotational speed, the strain rate had the most effect on the residual stresses whereas at the high rotational speed, some residual stress was released due to the generated heat in the weld zone.

ARTICLE HISTORY
Received: 14th Nov 2019
Revised: 29th June 2020
Accepted: 14th July 2020

KEYWORDS
Friction stir welding;
Residual stress;
Hole drilling strain gauge method;
Rotational speed;
Transverse speed

INTRODUCTION

The engineering properties of components, considerably such as fatigue life, distortion, dimensional stability, and brittle fracture can be significantly influenced by residual stresses which remain in parts after manufacturing process. Such common effects usually bring considerable costs in repairs and maintenances of components in engineering structures such as joining aerospace and marine structures [1] and need different joining method with high-tech inspections [2-6]. Consequently, residual stress analysis is a necessary stage in the design of welded components. One of the most applicable developed welding process of the last decade is Friction Stir Welding (FSW). FSW is a solid state process which was presented in 1991 by TWI and has potential to weld a wide range of structural materials, particularly difficult-to weld high strength Al/Mg alloys [7]. This mechanical process is designed based on the rotating tool which is inserted into the adjoining edges of the plates to be welded with a suitable tilt angle, and then moved along the joint. Due to the friction forces provided by the welding tool, both the metal flow behavior and the heat generated can be changed strongly [8]. Liu et al. [9] studied the influences of the manufacturing process parameters on the dimension of some micro-structural zones in the transverse direction of the welded joints. Ramulu et al. [10] studied the effect of tool rotational speed and feed rate on the forming limit of friction stir welded Al alloy sheets. Shigematsu et al. [11] investigated the effect of the material properties and Lee et al. [12] studied the mechanical effect caused by the grain refinement in the weld joints. In FSW process, both tensile and compressive residual stresses can be generated within the joint zone. The maximum residual stresses are placed in the heat affected zone which leads to phase transformation in this area [13], and the minimum residual stresses are positioned on the advancing side beyond the weld joint [1]. Krishna et al. [14] evaluated the effect of using the different tool pin profile of friction stir welding on the mechanical properties of Al plates. They concluded that the better mechanical properties of welded joint can be obtained by employing square tool. During the past years, several methods are introduced for assessment of residual stresses in different types of components. Zhan et al. [15] employed layer ultrasonic technology to study manufacturing parameters such as tool rotational speed on residual stress in FSW process. Dawson et al. [16], measured tensile and transverse residual stress distribution by neutron diffraction in the thermo-mechanically affected zone of the weld. Another relevant contribute was presented by Peel et al. [17], who used X-ray measurements to achieve the residual stress field in friction stir welded aluminum sheets at the different tool transverse speed. Similar studies were carried out by Staron et al. [18] and Jimenez-Mena et al. [19]. Another popular method for measurement of residual stresses is Hole-drilling method which is a semi-nondestructive mechanical technique for evaluation of magnitude, distribution and direction of residual stresses around the welding line. In this method a small hole would be employed at the location where the residual stresses are to be measured and the released strains on the surface are measured by the strain gauges bonded around the hole. Then, the residual stresses are calculated using a strain gauge rosette technique [20, 21]. In the last decades, many studies were carried out on the numerical simulation of FSW method. Song et al. [22], as well as Pashazadeh et al. [23] performed numerical models consider the heat of welding process caused by both friction forces and material deformation work. The model extended by Chen et al. [24], as well as Fratini et al. [25] using the commercial FEM software.

*CORRESPONDING AUTHOR | Mohammadreza Farahani | ✉ mrfarahani@ut.ac.ir

According to our best knowledge, less attention has been paid to study the effect of the both rotational and transverse speeds on the residual stress of FSW joints and thus, there was need further study. In the present study, the effect of above-mentioned parameters, on the residual stresses in FSW of aluminum plates is investigated. This work was performed by numerical analysis and the predicted results of residual stresses were compared with the results of hole drilling strain gauge measurement method.

FINITE ELEMENT ANALYSIS

Geometry, Mesh and Boundary Conditions

The numerical models were conducted by means of the finite element software package Abaqus [26]. Overall geometry was including two parts. Tool and plate. The tool was comprised of shoulder and pin. Upper and lower diameter of the shoulder were d_1=16mm and d_2=14mm with heights of h_1=42mm and h_2 =11mm, respectively. The pin of the tool had a square section with the length of a= 4mm and height of h_3=3.85mm. The tool was modeled as a discrete rigid body and a small fillet edges with radius of r= 0.2mm was considered on the sharp edges of the pin. In the present study, the FSW was performed on the AL 2024-T6. Its chemical composition is listed in Table 1. The plate with a length w_1= 40 mm, the width w_2= 20mm and the height h_4= 4 mm was employed. The general geometry of the plate and tool are shown in Figure 1(a) and (b), respectively. In the present research, the 3D thermo-mechanically coupled FEM model was used. Mass density and thermal conductivity of the plate were considered equal to ρ=2780Kg.m^3 and K=151 W.m^{-1}.k^{-1}, respectively. The elastic properties of this alloy and the other mechanical properties versus the temperatures are presented in ref. [27].

Table 1. Measured chemical composition of AL 2024-T6 (all elements are in weight percent)

Al	Mg	Mn	Fe	Si	Cu
92.115	1.57	0.613	0.284	0.0973	5.32

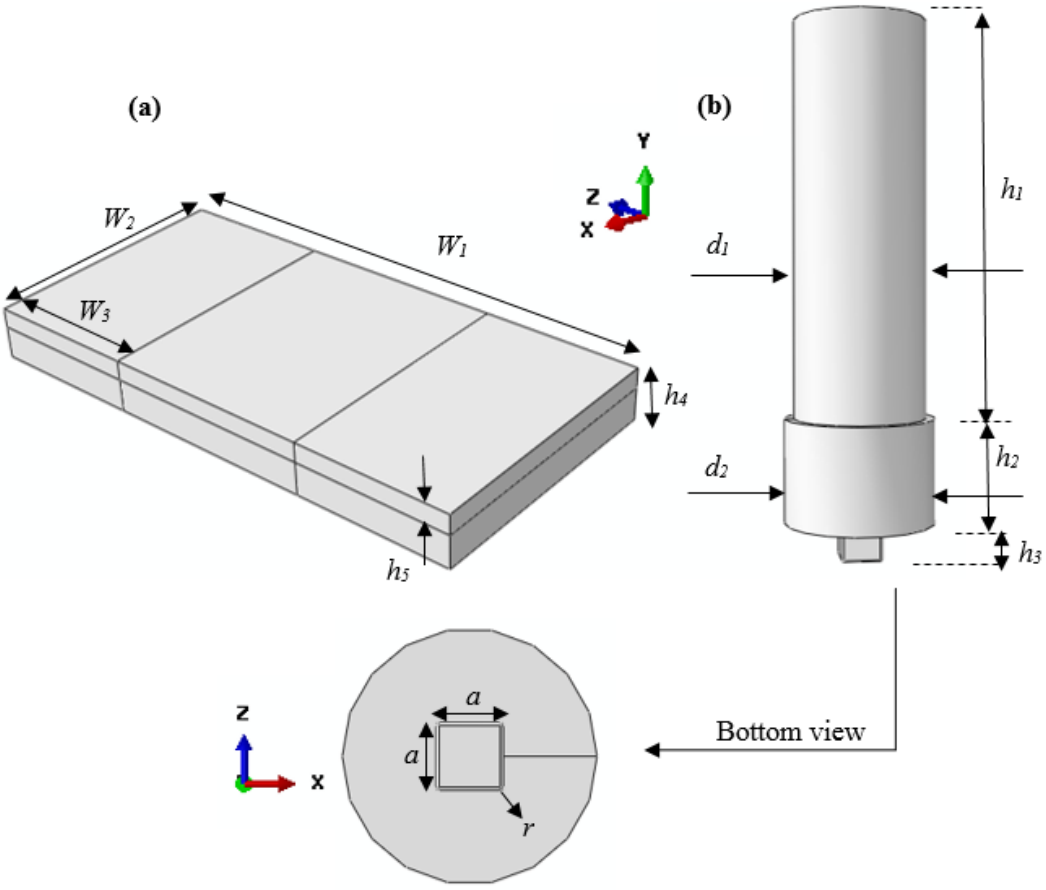

Figure 1. Sketch of the used: (a) plate (b) tool geometries

The proper tilt angle of the tool was kept constant equal to θ=3°. The process technological parameters of the tool were tool rotational and transverse speeds which were employed equal to 1120rpm, 1600rpm and 25mm/min, 31.5mm/min, respectively. The specific heat of the plate at room temperature was defined as a predefined field equal to C_p= 875J °C^{-1} kg^{-1}. In FSW process, the plates were clamped on the sides by pressure screws and supported in the bottom by a back plate, as depicted in Figure 2. These boundary conditions were modeled in FE simulation. Numerical simulation was performed in three stages. Rotational stage, penetration and displacement stage. Three amplitudes with tabular type were defined for every stage. The step time (t) was considered 25s in simulation. The plate was meshed with an 8-node thermally coupled brick, trilinear displacement and temperature, reduced integration (C3D8R). First order reduced integration elements of C3D8R have only one integration point and when subjected to deformation, the stress at the single integration point will be zero resulting in an element with no stiffness. To resolve this issue, an hourglass control with combined Visco-stiffness value was used that generates some artificial hourglass stiffness. The mesh sensitivity analysis was carried out in a way to find a good accuracy through the increase of the number of elements around the welding line. Base on this analysis, the mesh element size in the welding zone was selected 0.32mm × 0.19mm. Therefore, the plate was divided into several segments in numerical model by definition of datum planes (w_3= 12mm and h_5= 1.5mm which was chosen based on the depth of tool penetration) and the mesh was refined in the top-middle partition. The general meshing of the plate is shown in Figure 3.

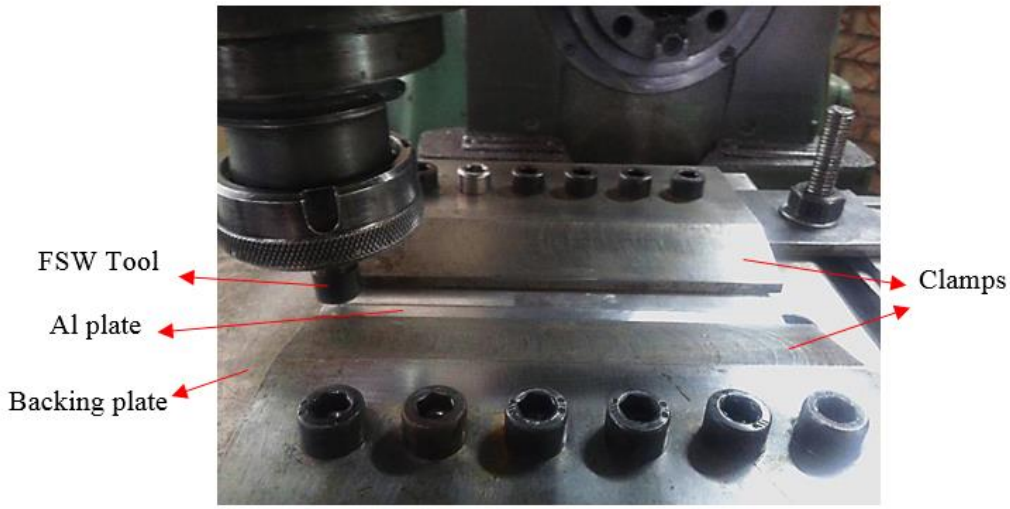

Figure 2. FSW process on the AL2024-T6

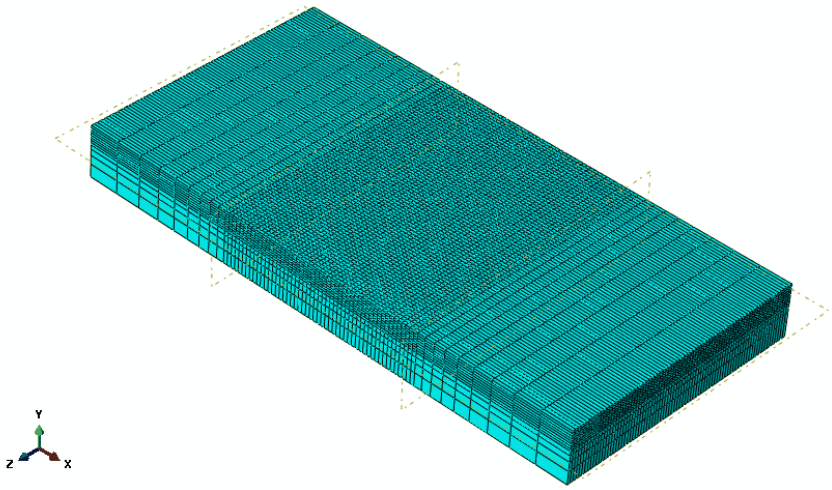

Figure 3. The sketch of the generated mesh in the plate

Residual Stress Measurement Method

The residual stress measurements were conducted in accordance with the procedure presented in the ASTM E837 standard [28]. Firstly, the surface of the workpiece was cleaned by the acetone. For the residual stress measurement, a rosette strain gauge was attached to the weld centerline of the workpiece. Then, a circular measurement hole drilled in the center of the gauge. This hole was made by very high speed carbide drill successfully. During the hole drilling process,

the value of the released strain was measured using strain gauge rosette as shown in Figure 4(a). A schematic view of hole drilling strain gauge is demonstrated in Figure 4(c), where D indicates the gauge circle diameter (5.13mm) and D_0 is the diameter of the drilled hole. According to the ASTM E837 standard, D_0 should lie within the range of 0.3–0.5D and the maximum depth should be 0.4D. The corresponding strain values (i.e. ε_1, ε_2 and ε_3) identified by the strain gauge are substituted into Eq. (1) to obtain the values of the minimum and maximum principal residual stress (σ_{min}, σ_{max}) [8]. In Eq.(1), A and B are material-dependent coefficients, whose values are derived directly from the tables presented in ASTM E837 in accordance with Young's modulus and Poisson's ratio of the specimen and the diameter of the drilled hole.

$$\sigma_{\min,\max} = \frac{\varepsilon_1 + \varepsilon_2}{4A} \mp \frac{1}{4B}\sqrt{(\varepsilon_3 - \varepsilon_1)^2 + (\varepsilon_3 + \varepsilon_1 - 2\varepsilon_2)^2} \quad (1)$$

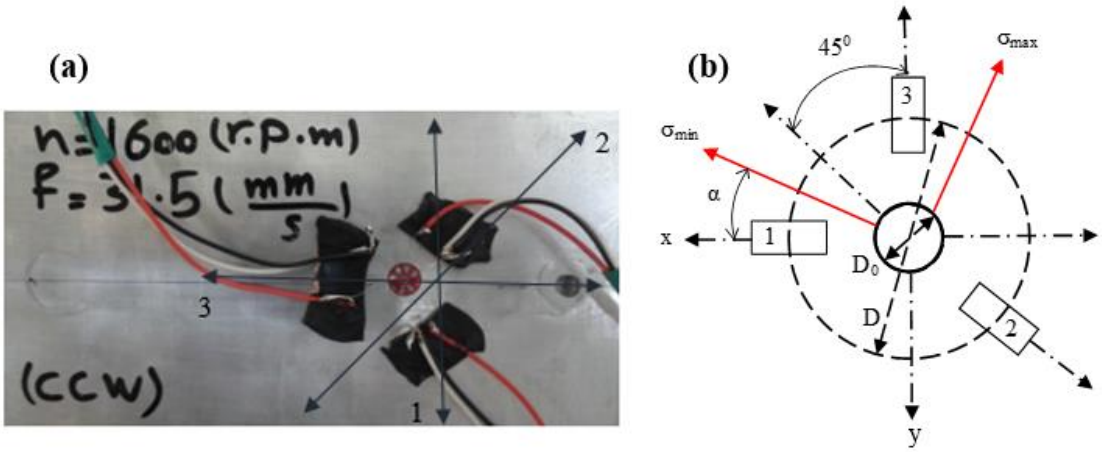

Figure 4. (a) Rosette strain gauge for residual stress measurement placed on the welding line before the test: (b) a schematic view of the hole drilling strain gauge method

RESULS AND DISCUSSIONS

The process parameters of the FSW process were considered based on the experimental design. In experimental design, each factor was set between the high and the low levels [29-31]. The process parameters of the FSW process were considered based on the experimental design. In experimental design, each factor is set between the high and the low levels. The factors were rotational speed and transverse speed of the tool in which rotational speeds and transverse speeds were employed as described in section 2.1. The prepared specimens were inspected visually. In order to check the reproducibility of the process, two specimens were manufactured for each experimental condition.

Temperature Distribution

Temperature distribution and progression for welding conditions identified by tool rotational speed of 1120rpm and tool transverse speed of 25mm/min are shown in Figure 5(a) to (c). During the sinking stage the maximum temperature about 285˚C was reached once the tool was prolonging in the feed direction. The obtained temperature for this model were already verified through the experimental results [32]. Temperature evaluations for different rotational speed at the same transverse speed of 25 mm/min which obtained from the simulation results are shown in Figure 6. It can be seen that the increase in the tool rotational speed has caused an increase in the peak temperature of the specimen up to 310˚C. Based on the experimental temperature analysis in FSW process [33, 34], the maximum temperature of the FSW process was seen between the 0.60 to 0.85 melting temperature (T_M) of base metal. The T_M of the AL2024-T6 substrate is 502˚C according to the manufacturer datasheet [35]. The results of this study also have showed the maximum temperature occurred in the ranges of 0.65 to 0.85T_M (see Figure 6). The absence of melting phenomenon decreased the temperature gradient as one of the main factors in residual stresses formation. In other words, the dough joined zone between the substrates tends to release more residual stresses due to equilibrium cooling conditions when compared to the fusion welding methods [36].

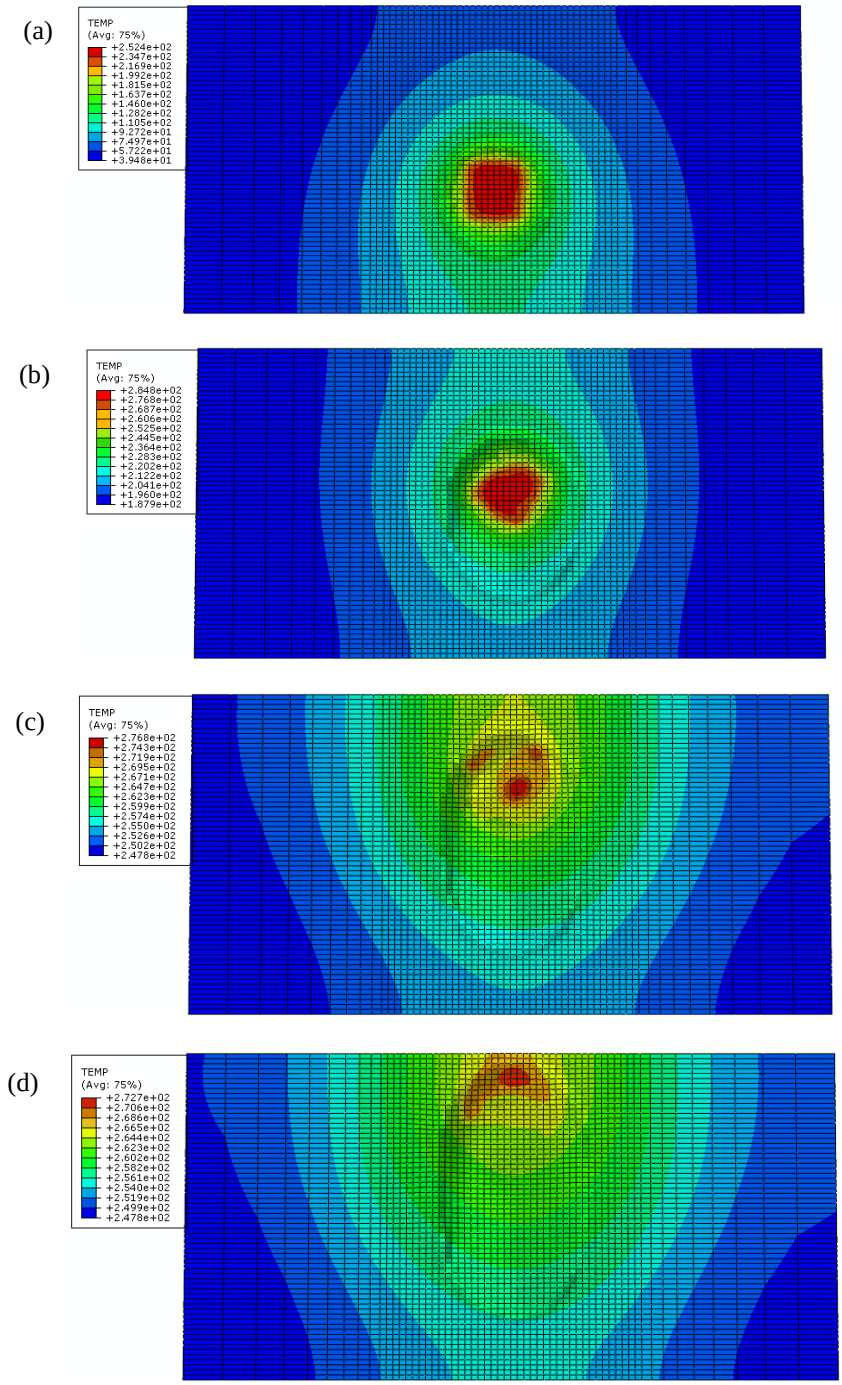

Figure 5. Illustration of temperature propagation of welding process (R.S. 1120rpm and T.S. 25mm/min case study)

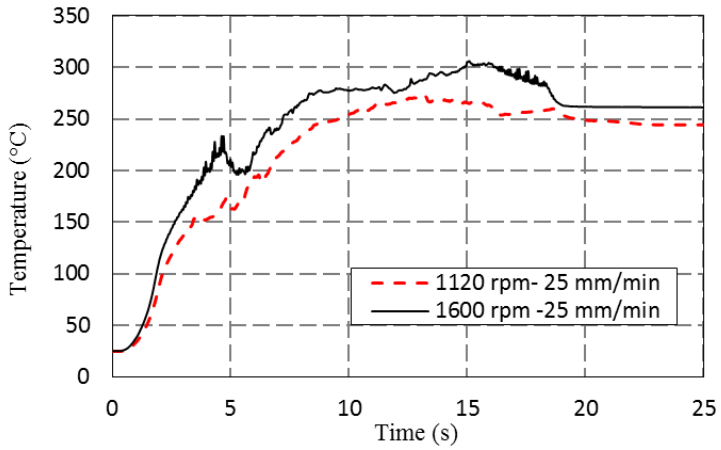

Figure 6. Temperature versus time of a point on the surface of the welding line

Residual Stress Distribution

The longitudinal and transverse residual stresses were calculated in three points by hole drilling strain gauge method in each sample. They were measured in weld centerline, retreating and advancing side as it is shown in Table 2. Tensile longitudinal residual stress was obtained for each sample. The result of this table was showed that the maximum residual stress value was 110.2MPa in the longitudinal direction in advancing side. This value was 32% of the yield strength of base metal. In the fusion welding processes, this value is about 90-95% of the yielding strength of the plate. Since the generated heat in FSW process was very smaller than of that in fusion welding, then the obtained value was reasonable. Finally, by keeping the mechanical constraint, the residual stress was generated after welding process and cooling down to room temperature. According to table 2 the largest values of residual stresses are founded parallel to the welding line in advancing side. This result was in accordance wih the study presented by Li et al. [37]. FEM longitudinal residual stress distribution on the top surface of the welding joint for 1120rpm and 2 mm/min case study is shown in Figure 7. It can be seen that, when the welding process reaches its steady state, a tensile stress is found in the weld zone. It was observed from the numerical simulation that the amount of the longitudinal residual stresses is greater at the periphery of the joint as confirmed by experimental results in Table 2.

Table 2. Residual stress obtained from the hole drilling strain gauge method

Specimen	Longitudinal Residual Stress (MPa)		
	Retreating Side	**Weld Centerline**	**Advancing Side**
R1120-T25	67.3	57.7	79.1
R1120-T31.5	69.6	60.71	95.5
R1600-T25	84.9	74.9	92.1
R1600-T31.5	85.2	76.7	110.2
	Transverse Residual Stress (MPa)		
	Retreating Side	**Weld Centerline**	**Advancing Side**
R1120-T25	-34.6	-55.2	-35
R1120-T31.5	-20	-34.1	8.3
R1600-T25	-64.3	-77.9	-53.1
R1600-T31.5	-32.3	-39.8	1.5

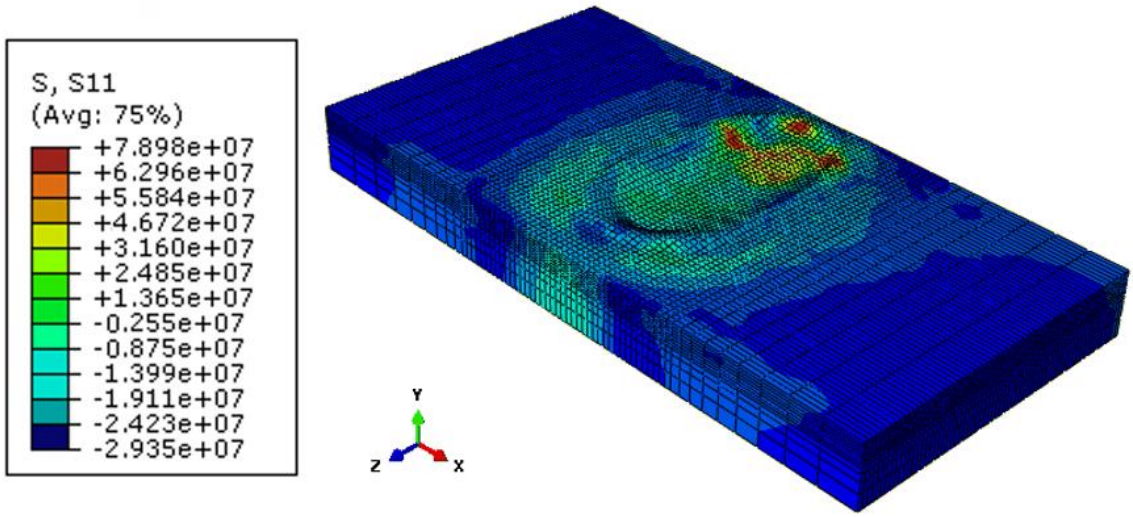

Figure 7. Longitudinal residual stress distribution caused by FSW process 1120rpm and 25mm/min case study

For more investigation, longitudinal and transverse residual stress profiles obtained from the numerical model were compared with the experimental results in Figures 8 and 9, respectively. In these figures, residual stress distribution at the retreating and advancing side with the distance of 8 mm from the welding centerline have been compared with the experimentally measured residual stress by the hole drilling strain gauge method. The residual stress calculated curves obtained from numerical model were in good agreement with the experimental results. As it was expected, larger longitudinal residual stress values are characterized for the welding condition of 1600rpm and 31.5mm/min. This result was in accordance with the outcome of the Jata et al. [38], they showed that the longitudinal stresses are always higher than the transverse residual stresses and exhibit an "M" like distribution. The maximum residual stress value was achieved about 110MPa, both in numerical model and experimental measurement (Figure 8). Besides, transverse residual stress in numerical model and experimental study displayed the negative values as presented by other studies [18, 39].

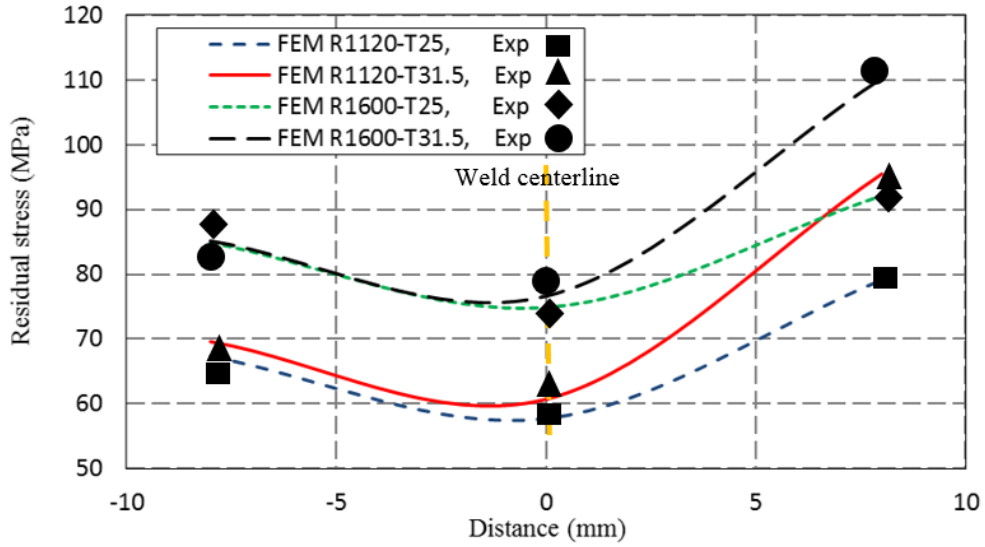

Figure 8. Numerical vs. experimental longitudinal residual stress distribution of the FSW process

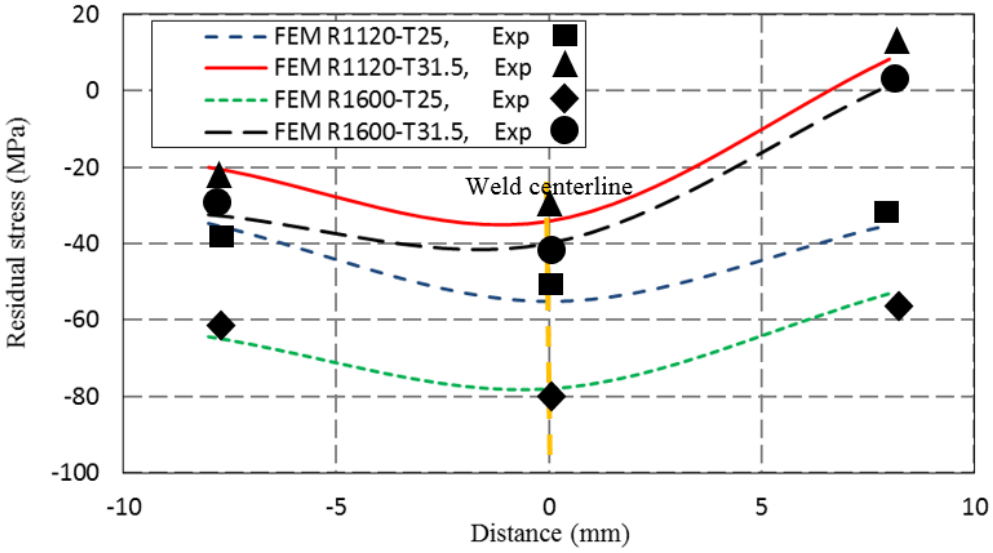

Figure 9. Numerical vs. experimental Transverse residual stress distribution of the FSW process

Based on the residual stress values which were obtained from the experimental and FE simulation, the effect of the tool rotational speed and transverse speed on the longitudinal residual stresses in the welding centerline are described by statistical analysis in the following. As depicted in Figure 10, the increase in rotational speed led to enhancement in the average residual stresses from 58.2 to 75.4MPa (29.55%). This increase in the amount of residual stresses may be caused by the greater temperature at higher tool rotational speed (see Figure 6). Additionally, it can be seen from the Figure 8 that the increase of the tool transverse speed led to enhancing of the average residual stresses from 65.34 to 68.7MPa (5.14%). This increase induced from more sever plastic deformation and higher strain rate at higher transverse speed. In other words, non-equilibrium cooling phenomenon was occurred in this situation. In non- equilibrium cooling cycle, the heat affected zone doesn't have the opportunity to release the stresses. This causes shrinkage in base metal and shrinkage forces tend to cause a degree of distortion, but due to embedded fixtures or boundary conditions surrounded metal substrates, the deformations restored as residual stresses in welding zone [40]. Additionally, the effectiveness of tool rotational speed on the magnification of the longitudinal residual stress was three times greater than that of tool transverse speed (see Figure 10(a) and (b)).

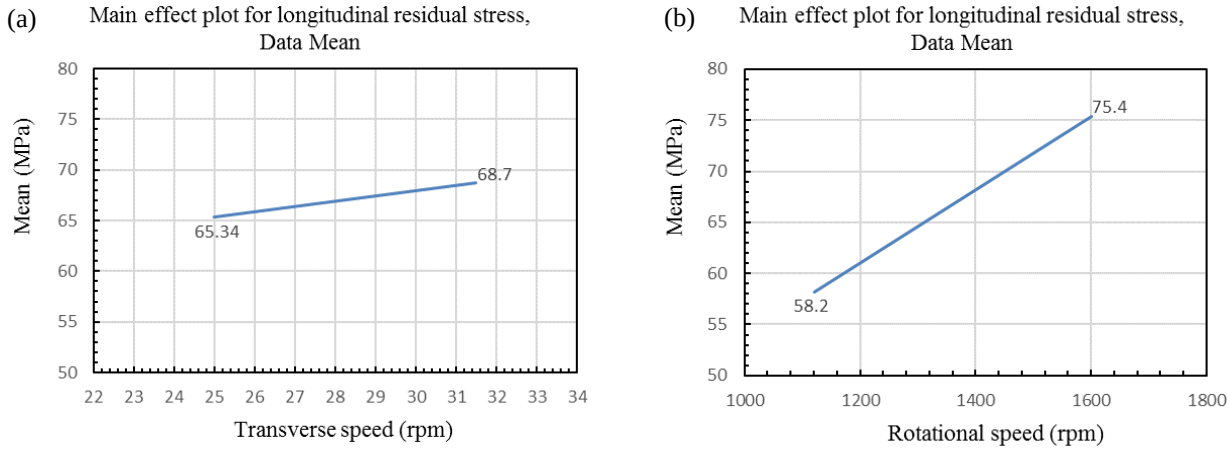

Figure 10. Main effect plot of the (a) tool transverse speed and (b) rotational speed on the longitudinal residual stress

Interaction effect of two factors, i.e. tool rotational speed and transverse speed on the mean longitudinal residual stresses is shown in Figure 11. The increase in longitudinal residual stress value was seen from 56 to 63MPa at 1120 rpm (12.5%) and from 75 to 77MPa at 1600 rpm (2.67%). No meaningful interaction effect between the tool rotational and transverse speed was observed.

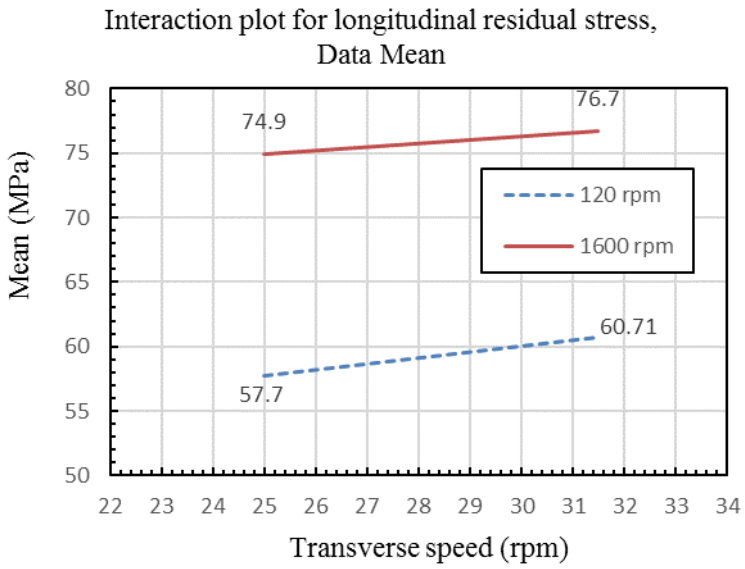

Figure 11. The interaction effects of the transverse speed and rotational speed on the longitudinal residual stress

CONCLUSIONS

In the present study, numerical and experimental work was carried out to evaluate the residual stresses induced from FSW process. The effect of the tool transverse and rotational speeds on the residual stress and temperature distribution across the weld line was studied. The most important results which were obtained from this study are listed as follows:

1) The heat rising around the welding line induced from an increase in the tool rotational speed led to increase in the longitudinal residual stress from 58.2MPa to 75.4MPa.
2) Due to strain rate rising around the welding line induced from an increase in the tool transverse speed caused an increase in the longitudinal residual stress from 65.34MPa to 68.7MPa.
3) The influence of the tool rotational speed on the magnification of the longitudinal residual stress in the weld centerline was three times more than the effect of the tool transverse speed.
4) The maximum residual stress was obtained 102.9MPa in the longitudinal direction in the advancing side for process parameters of 1600rpm- 31.5mm/min.
5) e) The interaction plot for longitudinal stress revealed that more rotational speed displayed greater residual stresses. It can be described that in lower rotational speed the strain rate was main factor on the residual stress whereas in higher rotational speed, the generated heat had a significant effect on the residual stress.
6) The behavior of this joint in the transverse direction is suitable for fatigue applications as transverse residual stress is negative in this direction.

ACKNOWLEDGEMENTS

This study was financially supported by The Welding and Non Destructive Testing Applied Research Center (TWN), University of Tehran. Additionally, the preparation of specimens, mechanical testing equipment and FE simulation were supplied by TWN.

REFERENCES

[1] R. S. Mishra and Z. Ma, "Friction stir welding and processing," *Materials science and engineering: R: reports*, vol. 50, pp. 1-78, 2005.

[2] O. Sam-Daliri, L.-M. Faller, M. Farahani, A. Roshanghias, A. Araee, M. Baniassadi, *et al.*, "Impedance analysis for condition monitoring of single lap CNT-epoxy adhesive joint," *International Journal of Adhesion and Adhesives*, vol. 88, pp. 59-65, 2019.

[3] C. Stetco, O. Sam-Daliri, L.-M. Faller, H. Zangl, "Piezocapacitive sensing for structural health monitoring in adhesive joints," in *2019 IEEE International Instrumentation and Measurement Technology Conference (I2MTC)*, 2019, pp. 1-5.

[4] O. Sam-Daliri, M. Farahani, L.-M. Faller, H. Zangl, "Structural health monitoring of defective single lap adhesive joints using graphene nanoplatelets," *Journal of Manufacturing Processes*, vol. 55, pp. 119-130, 2020/07/01/ 2020.

[5] G. Palardy, H. Shi, A. Levy, S. Le Corre, I. F. Villegas, "A study on amplitude transmission in ultrasonic welding of thermoplastic composites," *Composites Part A: Applied Science and Manufacturing*, vol. 113, pp. 339-349, 2018.

[6] T. Zhao, G. Palardy, I. F. Villegas, C. Rans, M. Martinez, R. Benedictus, "Mechanical behaviour of thermoplastic composites spot-welded and mechanically fastened joints: A preliminary comparison," *Composites Part B: Engineering*, vol. 112, pp. 224-234, 2017.

[7] O. Klag, J. Gröbner, G. Wagner, R. Schmid-Fetzer, D. Eifler, "Microstructural and thermodynamic investigations on friction stir welded Mg/Al-joints," *International journal of materials research*, vol. 105, pp. 145-155, 2014.

[8] D. Akbari, M. Farahani, N. Soltani, "Effects of the weld groove shape and geometry on residual stresses in dissimilar butt-welded pipes," *The Journal of Strain Analysis for Engineering Design*, vol. 47, pp. 73-82, 2012.

[9] G. Liu, L. Murr, C. Niou, J. McClure, F. Vega, "Microstructural aspects of the friction-stir welding of 6061-T6 aluminum," *Scripta materialia*, vol. 37, pp. 355-361, 1997.

[10] P. J. Ramulu, S. V. Kailas, R. G. Narayanan, "Influence of tool rotation speed and feed rate on the forming limit of friction stir welded AA6061-T6 sheets," *Proceedings of the Institution of Mechanical Engineers, Part C: Journal of Mechanical Engineering Science*, vol. 227, pp. 520-541, 2013.

[11] I. Shigematsu, Y.-J. Kwon, K. Suzuki, T. Imai, N. Saito, "Joining of 5083 and 6061 aluminum alloys by friction stir welding," *Journal of Materials Science Letters*, vol. 22, pp. 353-356, 2003.

[12] W. B. Lee, Y. Yeon, S. Jung, "The improvement of mechanical properties of friction-stir-welded A356 Al alloy," *Materials Science and Engineering: A*, vol. 355, pp. 154-159, 2003.

[13] S. Y. Betsofen, V. Lukin, M. Dolgova, M. Panteleev, Y. A. Kabanova, "Phase Composition, Texture, and Residual Stresses in Al–Cu–Li Friction Stir Welds," *Russian Metallurgy (Metally)*, vol. 2018, pp. 359-366, 2018.

[14] M. Krishna, K. Udaiyakumar, D. M. Kumar, H. M. Ali, "Analysis on effect of using different tool pin profile and mechanical properties by friction stir welding on dissimilar aluminium alloys Al6061 and Al7075."

[15] Y. Zhan, Y. Li, E. Zhang, Y. Ge, C. Liu, "Laser ultrasonic technology for residual stress measurement of 7075 aluminum alloy friction stir welding," *Applied Acoustics*, vol. 145, pp. 52-59, 2019.

[16] H. Dawson, M. Serrano, S. Cater, P. Wady, T. Pirling, E. Jimenez-Melero, "Residual stress distribution in friction stir welded ODS steel measured by neutron diffraction," *Journal of Materials Processing Technology*, vol. 246, pp. 305-312, 2017.

[17] M. Peel, A. Steuwer, M. Preuss, P. Withers, "Microstructure, mechanical properties and residual stresses as a function of welding speed in aluminium AA5083 friction stir welds," *Acta materialia*, vol. 51, pp. 4791-4801, 2003.

[18] P. Staron, M. Kocak, S. Williams, A. Wescott, "Residual stress in friction stir-welded Al sheets," *Physica B: Condensed Matter*, vol. 350, pp. E491-E493, 2004.

[19] N. Jimenez-Mena, T. Sapanathan, J. Drezet, T. Pirling, P. Jacques, A. Simar, "Residual stresses of friction melt bonded aluminum/steel joints determined by neutron diffraction," *Journal of Materials Processing Technology*, vol. 266, pp. 651-661, 2019.

[20] V. Dattoma, M. De Giorgi, R. Nobile, "On the residual stress field in the aluminium alloy FSW joints," *Strain*, vol. 45, pp. 380-386, 2009.

[21] A. Olabi and M. Hashmi, "Stress relief procedures for low carbon steel (1020) welded components," *Journal of materials processing technology*, vol. 56, pp. 552-562, 1996.

[22] M. Song and R. Kovacevic, "Thermal modeling of friction stir welding in a moving coordinate system and its validation," *International Journal of machine tools and manufacture*, vol. 43, pp. 605-615, 2003.

[23] H. Pashazadeh, J. Teimournezhad, A. Masoumi, "Numerical investigation on the mechanical, thermal, metallurgical and material flow characteristics in friction stir welding of copper sheets with experimental verification," *Materials & Design*, vol. 55, pp. 619-632, 2014.

[24] C. Chen and R. Kovacevic, "Thermomechanical modelling and force analysis of friction stir welding by the finite element method," *Proceedings of the Institution of Mechanical Engineers, Part C: Journal of Mechanical Engineering Science*, vol. 218, pp. 509-519, 2004.

[25] L. Fratini, S. Pasta, A. P. Reynolds, "Fatigue crack growth in 2024-T351 friction stir welded joints: Longitudinal residual stress and microstructural effects," *International Journal of Fatigue*, vol. 31, pp. 495-500, 2009.

[26] H. Hibbit, B. Karlson, P. Sorensen, "ABAQUS version 5.5—Theory manual," *Pawtucket, RI*, 1995.

[27] A. S. M. Handbook, "CINDAS/USAF CRDA Handbooks Operation," *Purdue University, West Lafayette, IN*, 2000.

[28] A. Standard, "E837-08 Standard Test Method for Determining Residual Stresses by the Hole-drilling Strain-gage Method," *ASMT international, West Conshohocken, PA*, 2008.

[29] O. Daliri, M. Farahani, M. Farhang, "A combined numerical and statistical analysis for prediction of critical buckling load of the cylindrical shell with rectangular cutout," *Engineering Solid Mechanics*, vol. 7, pp. 35-46, 2019.

[30] O. Sam Daliri and M. Farahani, "Characterization of Stress Concentration in Thin Cylindrical Shells with Rectangular Cutout Under Axial Pressure," *International Journal of Advanced Design and Manufacturing Technology* vol. 10, pp. 133-141, 2017.

[31] O. Sam-Daliri, L.-M. Faller, M. Farahani, A. Roshanghias, H. Oberlercher, T. Mitterer, *et al.*, "MWCNT–epoxy nanocomposite sensors for structural health monitoring," *Electronics*, vol. 7, p. 143, 2018.

[32] G. Buffa, J. Hua, R. Shivpuri, L. Fratini, "A continuum based fem model for friction stir welding—model development," *Materials Science and Engineering: A*, vol. 419, pp. 389-396, 2006.

[33] P. Colegrove and H. Shercliff, "Experimental and numerical analysis of aluminium alloy 7075-T7351 friction stir welds," *Science and Technology of Welding and Joining*, vol. 8, pp. 360-368, 2003.

[34] W. Tang, X. Guo, J. McClure, L. Murr, A. Nunes, "Heat input and temperature distribution in friction stir welding," *Journal of Materials Processing and Manufacturing Science*, vol. 7, pp. 163-172, 1998.

[35] A. Association, "International alloy designations and chemical composition limits for wrought aluminum and wrought aluminum alloys," *Teal Sheets*, pp. 1-28, 2009.

[36] P. Lacki, Z. Kucharczyk, R. Śliwa, T. Gałaczyński, "Effect of tool shape on temperature field in friction stir spot welding," *Archives of metallurgy and materials*, vol. 58, 2013.

[37] T. Li, Q. Y. Shi, H. K. Li, W. Wang, Z. P. Cai, "Residual stresses of friction stir welded 2024-T4 joints," in *Materials Science Forum*, 2008, pp. 263-266.

[38] K. Jata, K. Sankaran, J. Ruschau, "Friction-stir welding effects on microstructure and fatigue of aluminum alloy 7050-T7451," *Metallurgical and materials transactions A*, vol. 31, pp. 2181-2192, 2000.

[39] G. Buffa, A. Ducato, L. Fratini, "Numerical procedure for residual stresses prediction in friction stir welding," *Finite elements in analysis and design*, vol. 47, pp. 470-476, 2011.

[40] Z. Feng, *Processes and mechanisms of welding residual stress and distortion*: Elsevier, 2005.